Engineering Structures 116 (2016) 148–162

Contents lists available at ScienceDirect

Engineering Structures

journal homepage: www.elsevier.com/locate/engstruct

Lateral impact response of the concrete filled steel tube columns with and without CFRP strengthening

A.S. Shakir [a,b], Z.W. Guan [a,c,*], S.W. Jones [a]

[a] School of Engineering, University of Liverpool, Liverpool L69 3GQ, UK
[b] College of Engineering, Civil Engineering Dept., Al Muthanna University, Al Muthanna Province, Iraq
[c] School of Civil Engineering and Transportation, South China University of Technology, Guangzhou, PR China

ARTICLE INFO

Article history:
Received 16 October 2015
Revised 24 February 2016
Accepted 29 February 2016
Available online 10 March 2016

Keywords:
Concrete filled steel tube column
Lateral impact
CFRP
Recycled aggregate concrete
Theoretical prediction

ABSTRACT

This paper presents a study on the dynamic response of normal or recycled aggregate concrete filled steel tube (NACFST and RACFST) columns subjected to lateral projectile impact and the effect of the Carbon Fibre Reinforced Polymer (CFRP) jacketing on the structural behaviour of those columns. Eighty four specimens were studied to investigate the influence of the tube length, configuration of the impactor, concrete type and local reinforcement on the dynamic response. The results indicate that both the RACFST and NACFST specimens have a similar deformation shape, and the impact resistance of the RACFST specimens is comparable to that of the NACFST. The results also show that the additional confinement of the CFRP reduces the global displacement for both the RACFST and NACFST specimens. In addition the concrete filling increases the maximum impact force by 217%, 182% and 157% respectively for the short, medium and long tubes. On the top of the extensive experimental work, theoretical approaches were proposed to predict the maximum load and the corresponding displacement for all the columns tested, providing reasonably good correlation with the experimental results. Using the analytical model developed, further studies were undertaken to investigate the effects of the tube geometry, material properties, impactor configuration and impact energy on the structural response of the concrete filled tube columns.

1. Introduction

Normal Aggregate Concrete Filled Steel Tubes (NACFST) are increasingly used in many structural applications, such as seismic-resistant construction, high buildings, bridge piers and offshore structures [1–3]. NACFST have more advantages than conventional reinforced concrete and steel structural members, namely the high speed of construction work resulting from the omission of formwork and reinforcing bars, low structural costs and conservation of the environment [4–6]. NACFST also offer good damping properties and excellent seismic resistance [7]. Moreover, NACFST have good fire resistance compared with ordinary reinforced concrete, which leads to a reduction in the use of fireproof materials [4,8].

Some research work was initially conducted to study the flexural behaviour of NACFST under bending [7,9–11]. Elchalakani et al. [12] undertook experiments on 12 specimens of NACFST under pure bending. The results showed that the energy absorption and ductility were enhanced and that flexural strength for the thin circular hollow section was improved by the concrete filling more than for the thicker ones. They presented a theoretical model to predict the ultimate bending strength for the circular NACFSTs, which was in a good agreement with the experimental data.

With the increasing volumes of construction and demolition waste, resulting from the rapid development of the construction industry, recycling concrete waste becomes necessary to preserve the environment and to conserve the natural resources of gravel and sand [13]. Many studies have been conducted to investigate the behaviour of RACFST columns under static and cyclic loading [13–17]. The bearing capacity of NACFST columns is slightly higher than that of RACFST [18]. The research showed that under axial and cyclic flexural loading the behaviour of the tubular columns filled with recycled aggregate concrete is similar to those columns filled with normal aggregate concrete [19].

The use of confining Carbon Fibre Reinforced Polymer (CFRP) jackets has become increasingly popular to repair or strengthen concrete columns [20]. It was found that the additional confinement provided by CFRP strips increased the bearing capacity of the column and delayed its local buckling [21]. Dong et al. [17]

* Corresponding author at: School of Engineering, University of Liverpool, Liverpool L69 3GQ, UK.
E-mail address: zguan@Liverpool.ac.uk (Z.W. Guan).

http://dx.doi.org/10.1016/j.engstruct.2016.02.047
0141-0296/

conducted a study to understand the structural behaviour of RACFST strengthened by CFRP under axial compression load. Three parameters were examined, i.e. the replacement ratio of recycled aggregate (0%, 50%), the outer diameter to thickness ratio (D/t), and the reinforcement ratio by CFRP (0%, 75% and 100%). The arrangements of CFRP adopted in their study contributed to an increase on the load carrying capacity by 80% and 37% for the fully and partially strengthened columns, respectively.

Experimental studies were conducted to investigate the behaviour of the unfilled and filled tubes under axial impact loading [22–25]. The behaviour of the hollow and polyurethane foam filled steel tubes under axial impact load was investigated by Reid [26]. It was found that the foam filled tubes had a better bearing capacity than the empty ones. The concrete filled tube specimen could hold its shape without crushing, in comparison to the hollow tube specimen that was crushed under the same loading [27].

During the service life, structures are likely to be subjected to dynamic and/or impact loadings. For example, bridge columns could be impacted by a vehicle or boat, high buildings could be attacked by aircraft, or flying objects due to an accidental explosion [28]. Effects of the lateral impact load on the unfilled and filled tubes were investigated with different filling materials and tube materials. Xiaoqing and Stronge [29] studied the impact damage on hollow, water and sand filled steel tubes hit by spherical missiles, which showed that the water and sand filling reduced the deflection and increased the stiffness. Nishida and Tanaka [30] investigated the perforation and cracks of water filled aluminium tubes impacted by six steel spherical indenters with different diameters. However, it was concluded that under the conditions adopted in their study, the wall strength of the tube was reduced due to filling with water.

In recent years, a number of studies on the impact behaviour of the NACFST members have been conducted through experimental work, theoretical work and finite element analysis [11,31–35]. Remennikov et al. [36] compared the behaviour of Rigid Polyurethane (RP) foam and concrete filled steel square tubes under lateral impact loading. They showed that the impact resistance of stainless steel was higher than that of mild steel and RP foam enhanced the energy absorption. Wang et al. [37] investigated the lateral impact performance of the concrete filled steel tube members. Twenty two specimens were tested with the main test parameters as the impact energy, the axial load level and the constraining factor. It was demonstrated that the lateral deflection and the impact force could be affected by the axial load. A study of three experimental series was conducted by Yousuf et al. [38–40]. They investigated the transverse impact resistance of the hollow and concrete filled mild and stainless steel square tube columns. The structural behaviour of those columns was also studied through finite element analysis. The numerical results were compared with the experimental results with a good agreement. They found that the impact strength was improved by using stainless steel columns and the axial compressive load influenced the static and impact strength, especially for the stainless steel tubes.

To date, there has been limited research on the behaviour of RACFST under lateral impact loadings. In addition, the structural behaviour of the strengthened RACFST columns with CFRP local reinforcement has not been investigated under lateral drop-weight impact, according to authors' knowledge. The aim of this research is to investigate the impact behaviour of the NACFST and RACFST with different L/D ratios and impactor configurations, also to study the influence of the partial CFRP strengthening on the impact force and the lateral deformation of the NACFST and RACFST columns. The current study includes the testing of eighty four specimens with four varying parameters, i.e. (1) the length of the tube, (2) the concrete type, (3) the diameter or the shape of the impactor, and (4) the (CFRP) reinforcement. Comparisons between the impact behaviour of NACFST and RACFST with different parameters are presented and discussed. The results show that the RACFST columns with a 50% replacement ratio of the recycled aggregate have a similar deformation mode to those with normal aggregate. The results also show that the CFRP reinforcement has some effects on the impact force and the global displacement. Furthermore, theoretical predictions of the maximum force and the related displacement of the columns are provided and compared with the experimental results, which show a good agreement. A series of parametric studies are further carried out to investigate the influence of various parameters on the structural behaviour of the columns.

2. Experimental programme

2.1. Materials

There are three materials used in this study: concrete, mild steel and CFRP. The average 28-day compressive strength of the normal and recycled aggregate concrete cubes tested, in accordance to the British Standard [41], were 56 MPa and 53 MPa, respectively. Ordinary Portland cement, river sand and coarse aggregate were used to produce the concrete. The coarse aggregate was in two categories, i.e. normal aggregate (NA) and recycled aggregate (RA). The recycled aggregate was supplied by Sloyan Doyle demolition company (Liverpool, England), which was obtained by crushing the concrete from demolished concrete structures. Both of the NA and RA had a maximum size of 10 mm. The density was 2627 kg/m^3 and 2558 kg/m^3 for NA and RA, respectively.

Cold formed steel tubes with a circular section were used to produce the specimens. The obtained yield and ultimate strength of steel from standard tensile coupon tests were 450 MPa and 542 MPa, respectively. The elastic modulus was 200 GPa and Poisson's ratio was 0.3.

A woven CFRP with a nominal thickness of 0.28 mm (2/2 twill) was used to strengthen the column. CFRP woven was supplied by "Easycomposites" (Staffordshire, England) with a density of 1390 kg/m^3. An Instron 4204 testing machine was used to conduct the tensile test of the CFRP. The tensile strength and modulus of elasticity obtained are 550 MPa and 48 GPa, respectively.

2.2. Mixing proportions

To minimise the effect of the high water absorption of the RA on the workability and the hydration of the concrete mix, the RA was pre-soaked for 24 h before the concrete mixing with an amount of water equal to 6.2% of the total weight of the RA. This percentage of water is calculated from the difference between the water absorption of the RA and NA, i.e. 7.40% and 1.18%, respectively. The free water–cement ratio was 0.46 for both mixes and the adopted replacement ratios of the recycled aggregate in this study were 0% and 50% of the total weight of coarse aggregate. Table 1 shows the details of the mix proportions for both the normal and recycled aggregate concrete, together with the slump measurements.

2.3. Preparation of specimens

Eighty four hollow and concrete filled steel tube specimens with an outer diameter (D) of 114.3 mm were prepared, which include 7 hollow tubes, 39 tubes filled with recycled aggregate concrete and 38 tubes filled with normal aggregate concrete. The specimens (excluding the hollow ones) were divided into five groups with the first four groups containing 14 tubes each, of which six tubes were strengthened with CFRP. The fifth group

Table 1
Mix promotions of recycled and normal aggregate concrete.

Concrete type	Replacement ratio (%)	Cement (kg)	Water (kg)	Sand (kg)	NA (kg)	RA (kg)	Slump (mm)
Normal	0	438	203	710	977	0	95
Recycled	50	438	203	710	489	489	89

includes 21 tubes to be subjected to impact by four different impactors without the CFRP strengthening. The tubes in the first group are with 3 mm wall thickness (t), whilst that for the other groups is 3.6 mm thick. To examine the effect of the specimen length on the impact response of the tubes, the specimens were prepared in three different lengths, i.e. 686 mm (6D), 1029 mm (9D) and 1543 mm (13.5D). The letters S, M, and L in the specimen ID refer to Short, Medium and Long, respectively. The "50" and "0" represent 50% of the recycled aggregate and the normal aggregate concrete, respectively. The small letter "s" refers to the strengthened tube with CFRP and the letter "H" refers to the hollow tube. To examine the effect of impactor shape on the behaviour of the CFST, two types of impactor were used in the tests. The first one is the spherical impactor with three diameters of 60 mm (BI), 40 mm (MI) and 20 mm (SI). The second type is a flat impactor with 40 mm × 40 mm square (FI) section.

The interior surface of each tube was cleaned by steel wire brush to remove any rust and/or dust. Each tube was filled with the concrete in layers and then compacted using a vibration poker. All the tubes were covered by a nylon sheet after the compaction to retain the necessary moisture to ensure complete hydration. The gap resulting from shrinkage at the top surface of the concrete was filled with cement mortar.

The bearing capacity and stiffness of the CFST columns strengthened with CFRP could be considerably enhanced [17]. The ductility of the columns increases with reducing the number of layers of CFRP reinforcement [42]. At the same time, CFRP is an expensive material. Thus, only one layer with a length equal to one-thirds of the tube length was used in this investigation. Strengthening the mid span area was adopted, as this area experiences a higher local and global displacements during the direct impact by a drop-hammer.

To obtain a better bond between the surface of the tube and the CFRP, the external surface of the steel tube was treated by a rough aluminium oxide paper and then cleaned by dry tissue to remove dust. EL2 epoxy laminating resin has a 100:30 mixing ratio, i.e. 100 parts of resin to 30 parts of hardener by weight was used. After the woven sheet and resin were placed on the tube, the tube was tightly wrapped by a high shrink composite tape to consolidate the strengthening. Post curing in an oven at up to 60 °C for 8 h was applied to help settlement for one layer of the reinforcing material as recommended by the manufacturer.

2.4. Set up of the impact test

The specimens were tested under lateral impact load using a drop-hammer, as shown in Fig. 1. The maximum height of the rig is 2.6 m. The mass of the drop hammer is 106, 106.5, 107, and 107.5 kg for SI, MI, FI, and BI respectively. High strength steel clamps were used to provide fixed ends of the specimens to mimic the fixed boundary conditions of the column ends. In order to reduce the vibration resulting from the high energy impact, a steel frame was used to fix the steel clamp to the ground with a 12 mm thick fiberboard. The clamps were adjustable on the steel frame to suit the change of the tube with different geometry. A Laser Doppler Velocimeter (LDV) was used to obtain the impact force and the total displacement. The Dantec Flowlite LDV system was adopted in this study. This system includes a Burst Spectrum Analyser enhanced (BSA) signal processor model 57N21, which was linked to a computer via an interface card, optic unit and a fibre optic cable. All the impact tests were carried out with the similar initial impact energy, which was 2650 J ± 100 J depending on the weight of the impactor and the initial velocity. To capture the total and global displacements and the mode of failure of the specimen, a High Speed Camera (HSC) was used with two high voltage lights. The LDV signals were processed using the digital filter software imPRESSion 6 [43] with 500 Hz cut-off frequency to smooth the noise. During each test, measurements of the velocity–time history and the deformations were recorded, and then the global displacement, the total displacement and the contact force were derived from the HSC and LDV. The permanent indentation was also measured using a Vernier caliper and steel strip.

3. Results and discussion

3.1. Load–displacement relationships

When the impactor hits the tube with an initial velocity, the deformation will start with a local indentation, as shown in Fig. 1 (c), which is equal to the deference between the displacement on the top surface (or the total displacement) and the displacement on the bottom surface (or the global displacement). Therefore, two types of displacements were obtained in this study using the high speed camera and the laser Doppler Velocimeter, i.e. the total displacement (δ) and the global displacement, as shown in Figs. 2–8 and in Figs. 9 and 10 respectively.

The concrete filling contributes to increasing the maximum impact force by 217%, 182% and 157% respectively for the short, medium and long tubes in comparison to their hollow counterparts. Furthermore, the concrete filling causes a significant reduction in the total and global displacements. For the short tube, the global and total displacements were reduced by 31% and 75%, respectively. The total displacement decreased by 68% for the tube with L/D ratio of 9, while it decreased by 75% for the one with L/D ratio of 13.5. The test results are summarised in Table 2.

Fig. 2 shows impact force – total displacement curves of the short, medium and long hollow steel tubes. The maximum force was increased from 64.74 kN for the long tube to 83.97 kN for the short one, while the corresponding maximum total displacement decreased from 68.7 mm to 52.1 mm. From these results, it can be seen that with increasing the tube length, the local deformation increases and the impact force decreases, as expected.

Fig. 3 reveals that the filling of the tube with concrete enhances the resistance to the local indentation and reduces the total displacement. Fig. 3 also shows that the maximum force decreases when the tube length increases. The maximum force for the concrete filled short tube is 266 kN, while it decreases by 27% and 38% for the medium and long tubes, respectively. The vibration effect is also evident for the long tube.

Fig. 4 gives the comparisons of the long tubes filled with normal or recycled aggregate with or without the local CFRP strengthening. The maximum force for the tube filled with normal aggregate was 166 kN, while that for the one filled with recycled aggregate was 164 kN, also with the displacement being increased from 28.2 mm to 29.8 mm. In general, for the specimens filled with recycled aggregate concrete, the maximum force was slightly lower

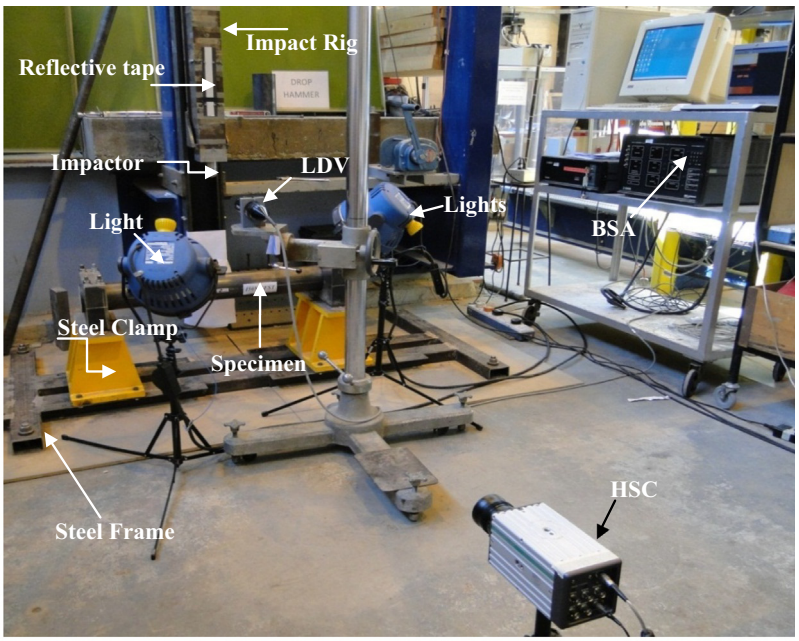

(a) General set-up

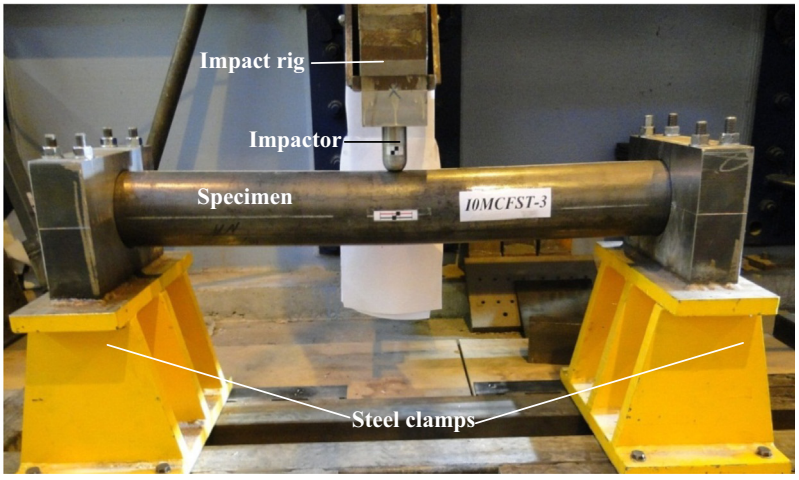

(b) Close up image

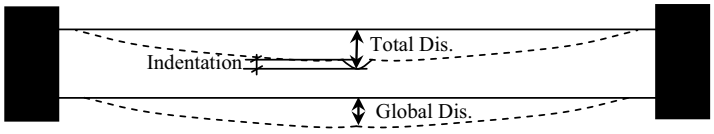

(c) The total and global displacements

Fig. 1. Set up of the impact test. (a) General set-up. (b) Close up image. (c) The total and global displacements.

than that filled with normal aggregate, whilst the displacement was higher. This is due to the lower mechanical properties of the recycled aggregate which leads to the slight reduction of the load carrying capacity of the concrete. The recycled aggregate has the same effect on the medium and short tube, as shown in Figs. 5 and 6, respectively. The contact force for the medium tube was reduced by 6.3%, while the reduction for the short tube was 6.4%. This evidence suggests that the RACFST columns can be used in the new construction with suitable quality control. Moreover, the tubes with the CFRP strengthening do show a higher initial stiffness.

The effect of the impactor shape on the impact behaviour of the CFST columns was examined. The results show that with the increasing size of the impactor, the contact force increased and the total displacement decreased for both types of concrete, as expected. Fig. 7 shows that increasing the diameter of the impactor from 20 mm to 60 mm leads to an increase of the contact force from 220 kN to 286 kN due to a larger contact area, while reducing the total displacement from 16.3 mm to 13 mm, respectively. The RACFST specimens give a lower bearing capacity than the NACFST specimens with different impactor shape and diameter, which is shown in Fig. 8. The load capacity of the RACFST specimen tested

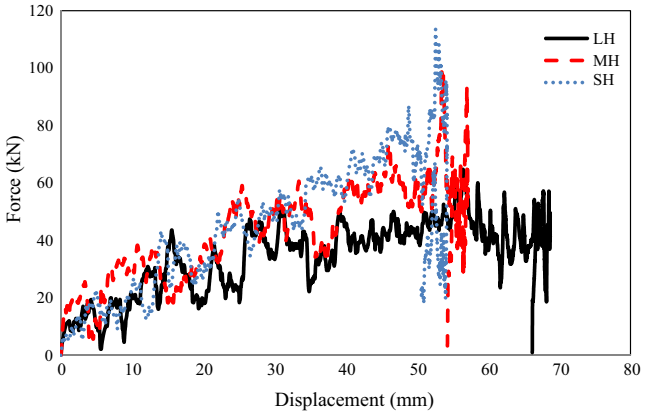

Fig. 2. The force–displacement curves for the hollow tubes with different lengths.

with the small impactor (SI) is reduced slightly from 220 kN to 216 kN, whilst those tested with medium impactor (MI) are reduced from 267 kN to 259 kN. The maximum force and the total displacement for the specimens tested are displayed in Table 2.

The strengthened NACFST and RACFST specimens with CFRP show a similar impact response; however, the contact forces for the strengthened tubes with three different lengths are less than those of the unstrengthened ones during the first stage of the test, as shown in Figs. 4–6. The use of one layer of CFRP caused a drop of the contact force, as it dampened the contact interaction and reduced the frequencies, which contributed to the reduction of the maximum force. From Fig. 4, it can be seen that the maximum force reduced for all the long specimens is from about 160 kN down to as low as 10 kN. This is likely attributed to the vibration of the specimens and bouncing back of the impactor during the test. However, the contact forces associated with the CFRP strengthened tubes were reduced less than those of the unstrengthened specimens due to the damping effect of the CFRP mentioned before. The contact force for the medium-long strengthened specimen was 176.7 kN, while it was 193.7 kN for the related unstrengthened specimen. The strengthened RACFST specimens exhibited the same behaviour to those with normal aggregate. The contact force was reduced from 164 kN to 142 kN for the long RACFST specimens.

The global displacement evaluated from the HSC for the strengthened NACFST and RACFST indicates that the CFRP has a reasonable effect on the global displacement of the tubes. Fig. 9 and 10 show that one layer of CFRP reduces the global displacement by about 8.3% and 6.2% for the long and medium tubes, respectively. It can be seen from the figures that the initial displacement is almost zero with sharp increasing contact force. This is because the initial local indentation is not being taken into account in the global displacement, which gives much higher initial stiffness on the load versus global displacement plots.

3.2. Deformation modes

Despite the columns being tested with three different L/D ratios, RACFST and NACFST columns failed in a similar deformation mode. The sequence of the failure is: (1) the local indentation is initiated at the contact area between the impactor and the column; and (2) the global deformation at the mid-span of the column begins when the impact energy exceeds the local deformation energy. Fig. 11(a) shows the effect of the specimen length on the local indentation mode. It can be seen that, with the same spherical impactor, the indentation diameter decreases with increasing specimen length, which are 18 mm for the long tube (L), and 21 mm and 25 mm, for the medium (M) and short (S) tubes, respectively.

The indentation depth was also measured with the average depth for the short tube as 6.2 mm, while 4.9 mm for the medium tube and 4.2 mm for the long tube. It is clear that the initial indentation increases with increasing tube stiffness which is dependent on the length of the specimens. With different diameters of the spherical impactor, the indentation diameter increases with impactor diameter as expected, whilst the indentation of the flat impactor has the same dimensions and shape of the impactor. The indentation depths of the small and medium impactors are 10.1 mm and 6.2 mm respectively, whilst that for the large

Table 2
The impact test results.

Specimen ID	Maximum force (kN)	Total disp. (mm)	Indentation (mm)	Total energy (J)	Absorbed energy (J)	Absorbed energy ratio* (%)
S0	217.3	19.0	11.9	2655.0	2460.0	92.7
S50	195.7	19.4	12.3	2670.0	2472.0	92.6
S0s	229.4	20.8	13.7	2661.0	2455.0	92.3
S50s	187.4	19.9	13.7	2578.0	2422.0	93.9
SH	84.0	52.2	–	2442.0	2268.0	92.9
S0-BI	286.3	12.9	4.6	2478.0	2152.0	86.8
S50-BI	259.3	13.4	5.2	2481.0	2217.0	89.4
S0-MI	266.0	14.0	6.2	2687.0	2340.0	87.1
S50-MI	250.0	14.6	6.4	2659.0	2314.0	87.0
S0s-MI	274.0	13.9	7.1	2522.0	2247.0	89.1
S50s-MI	253.0	14.0	7.1	2486.0	2199.0	88.5
S0-SI	220.1	16.4	10.2	2546.0	2308.0	90.7
S50-SI	216.0	15.6	10.4	2527.0	2277.0	90.1
S0-FI	319.0	11.2	1.9	2455.0	2191.0	89.2
S50-FI	317.8	11.4	2.2	2509.0	2214.0	88.2
MH	98.7	57.1	–	2460.0	2336.0	95.0
M0	193.0	18.8	4.9	2616.0	2182.0	83.4
M50	181.1	19.2	4.9	2653.0	2229.0	84.0
M0s	176.7	19.2	5.0	2470.0	2060.0	83.4
M50s	179.7	18.6	5.2	2445.0	2013.0	82.3
LH	64.7	68.7	–	2351.0	2253.0	95.8
L0	166.0	28.2	4.2	2643.0	2257.0	85.4
L50	164.1	29.8	4.3	2729.0	2449.0	89.7
L0s	132.5	29.0	4.8	2464.0	2095.0	85.0
L50s	142.1	28.0	4.9	2449.0	2084.0	85.1

* (Absorbed energy / Total energy) ×100.

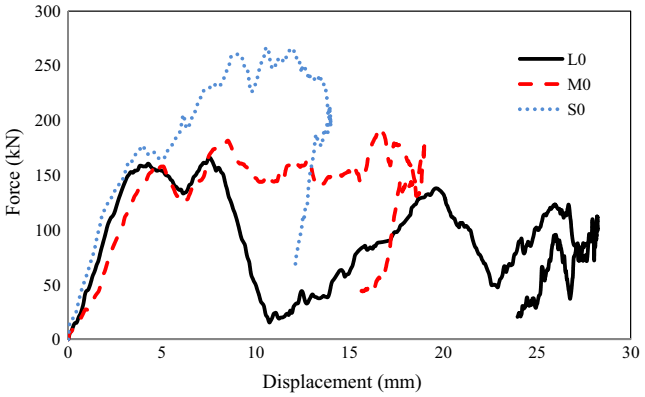

Fig. 3. The force–displacement curves for the concrete filled tubes with different lengths.

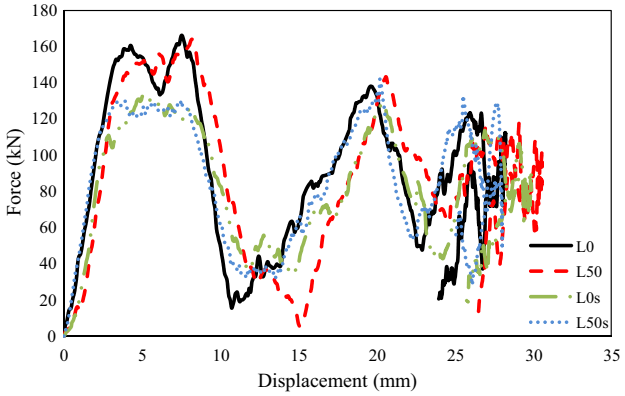

Fig. 4. The force–displacement curves for the long NACFST and RACFST tubes with and without CFRP strengthening.

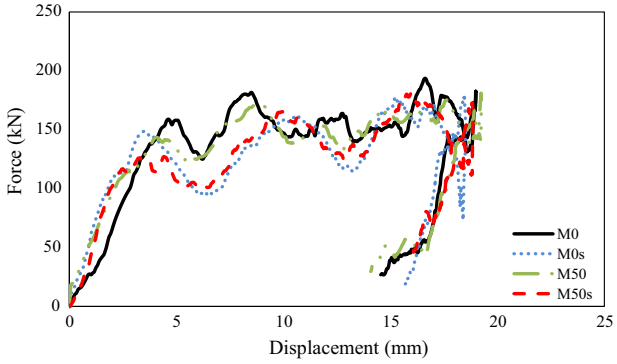

Fig. 5. The force–displacement curves for the medium NACFST and RACFST tubes with and without CFRP strengthening.

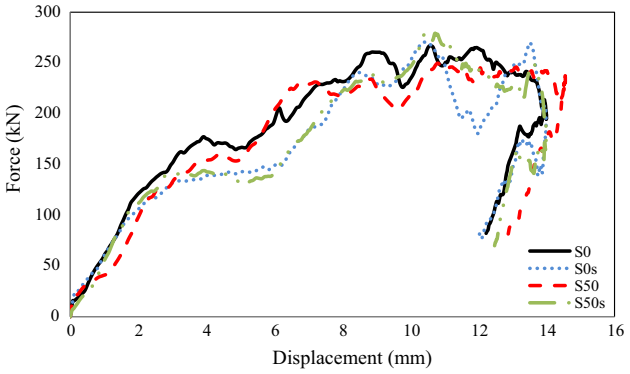

Fig. 6. The force–displacement curves for the short NACFST and RACFST tubes with and without CFRP strengthening.

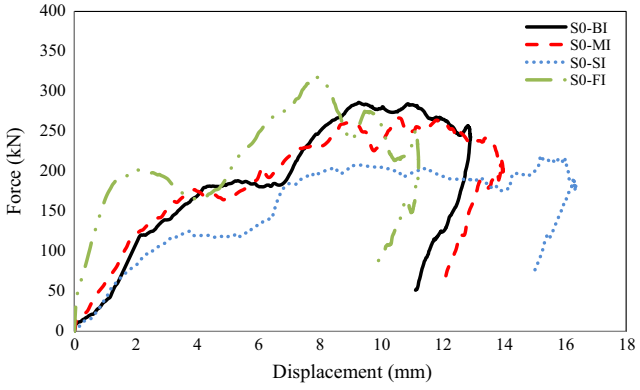

Fig. 7. The force–displacement curves for the short NACFST tubes with different impactors.

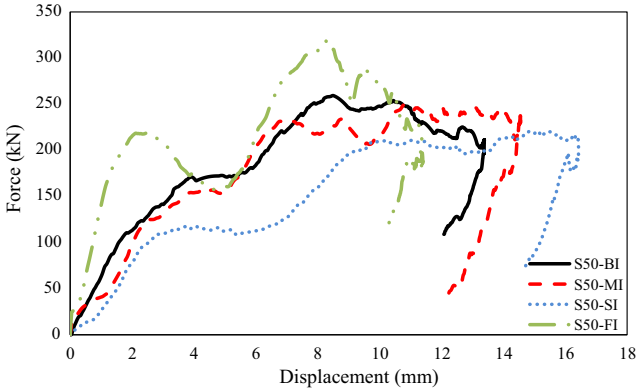

Fig. 8. The force–displacement curves for the short RACFST tubes with different impactors.

impactor is 4.6 mm and that for the flat impactor is only 1.85 mm. The effects of the diameter and the shape of the impactor are shown in Fig. 11(b).

For the specimens strengthened with CFRP, the failure of the surface reinforcement was initiated with a crack at the bottom of the section in the mid-span and around the edge of the indentation. The contact area of the CFRP layer with the impactor was completely smashed. However, there was no obvious separation observed between the CFRP layer and the steel tube, except for the contact area with the spherical impactor in a small diameter, as shown in Fig. 12. The effect of the specimen length can be clearly seen, with the crack width increased from 1 mm for the short tube to 5 mm for the long one and the crack width for the medium tube about 2 mm. Table 2 reveals that with one layer of CFRP reinforcement the indentation depth increased slightly for a given tube length, due to enhancement of the stiffness of the tube which gives a higher resistance to the global deflection.

Although concrete is a brittle material, the confinement effect allows the concrete to behave like a ductile material, as can be seen from Fig. 13, in which the indentation diameter and shape for the concrete core are shown. The cracks were initiated at the mid span of the concrete core opposite to the indentation side. With the

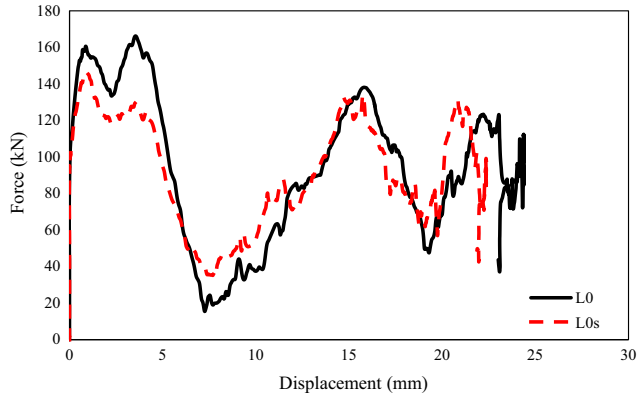

Fig. 9. The effect of the FRP layer on the global displacement of long CFST specimens.

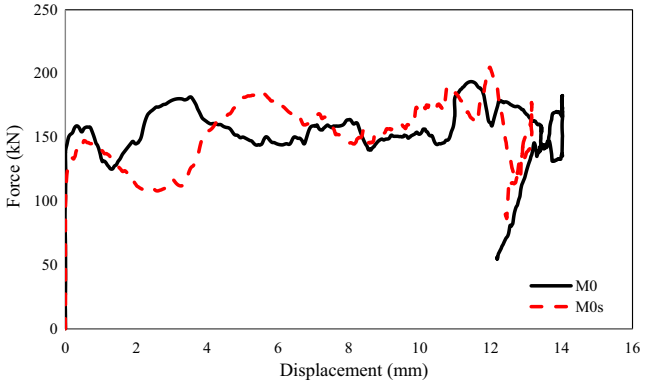

Fig. 10. The effect of the FRP layer on the global displacement of the medium CFST specimens.

increasing tube length, the crack width and the numbers of cracks were also increased due to a larger deflection.

Fig. 14 shows that the hollow steel tubes failed in a similar manner, despite there being three different lengths. The local indentation depth at the mid span of the short tube was higher than those of the medium and the long tubes, while the overall displacement was smaller. Fill the tube with concrete plays a vital role in changing the deformation mode of the specimens, also reducing the local indentation and the global displacements as well as avoiding local buckling due to the composite action of the concrete core and steel tube.

3.3. Energy absorption

The area beneath the force – displacement curve was used to calculate the total and absorbed energies, as can been seen in Fig. 15. The ratio of the energy absorption to the total energy applied was then determined, which are tabulated in Table 2. According to the test results, the total energy absorption was highly affected by the CFRP. The total energy absorption decreased from 2340 J to 2247 J for the short tubes without and with CFRP, whilst the reduction for the medium and long tubes were 6% and 8%, respectively. This is due to increasing the specimen stiffness, as a result of the additional confinement of one layer of CFRP. The effect of the D/t ratio on the energy absorption is clearly shown. The total energy absorbed by the short tube with a D/t ratio of 38 is 5% higher than the short tube with the ratio of 32. In general, the energy absorbed for the specimens filled with recycled aggregate concrete was slightly higher than those filled with normal aggregate concrete. The energy absorbed by the long tube with RA was 8.5% higher than those with NA, perhaps due to a relatively low strength of the RA concrete. As shown in Table 2, it can be seen that the hollow tube columns absorbed most of the applied impact energy, with a percentage of 93, 95 and 96% for the short, medium and long tubes, respectively. However, such the ratio for the CFST columns was reduced by 6%, 13% and 12%, respectively, due to the enhanced stiffness by the concrete core. In general, the tubes filled with RA and NA concrete exhibited the similar ratio of the energy absorption.

4. Modify the simplified analytical models

4.1. Total displacements

A simplified analytical model was developed to predict the maximum total displacement "δ_{max}" at the mid-span of the fixed-pin ended circular CFST column under impact loading [33]. The model assumes that the impact kinetic energy (KE) is dissipated by two plastic hinges formed at the maximum deflection of the mid-span of the column. The local deformation of the column is ignored in this model and the maximum total displacement can be predicted as follows:

$$\delta_{max} = \frac{L}{2} \times \theta \tag{1}$$

where L is the column length and θ refers to the rotation angle of the tube end, which can be obtained from:

$$\theta = \frac{\mathrm{KE}}{3M_p} \tag{2}$$

Here, M_p refers to the dynamic plastic moment of the column section which is calculated from the experimental sustained impact force based on the bending moment diagram with consideration of the strain rate effect for both steel tube and concrete core by using a dynamic enhancement factor.

Bambach [31] assumed three plastic hinges as a failure mechanism for the fixed ends CFSTs. In the current study, it is also assumed that the CFST tube with both ends fixed forms three plastic hinges as shown in Fig. 16, although they may not occur simultaneously. As the result of this fixity, the rotation angle is reduced. Therefore, Eq. (2) is modified to count for the extra constraint, which is proposed as

$$\theta' = \frac{\mathrm{KE}}{4M_p} \tag{3}$$

The impact kinetic energy can be calculated from:

$$\mathrm{KE} = \frac{1}{2}MV^2 \tag{4}$$

where M and V are the mass of the drop-hammer and its impact velocity, respectively. To predict the maximum total displacement of the CFST columns with fixed ends, Qu's model [33] was modified using a regression analysis. The modified model considers the effect of the impactor shape by introducing a shape factor "A", which is dependent on the ratio of the external tube diameter to the spherical impactor diameter (D/d_i) and the ratio of the tube length to the tube diameter (L/D). The shape factor can be expressed as

$$A_1 = \begin{cases} 0.1211 \times \frac{D}{d_i} + 1.75, & \text{for } 3 < \frac{L}{D} < 13 \\ 0.1211 \times \frac{D}{d_i} + 1.2, & \text{for } \frac{L}{D} \geqslant 13 \end{cases} \tag{5}$$

The shape factor for a flat impactor with a 40 mm × 40 mm square section is taken as:

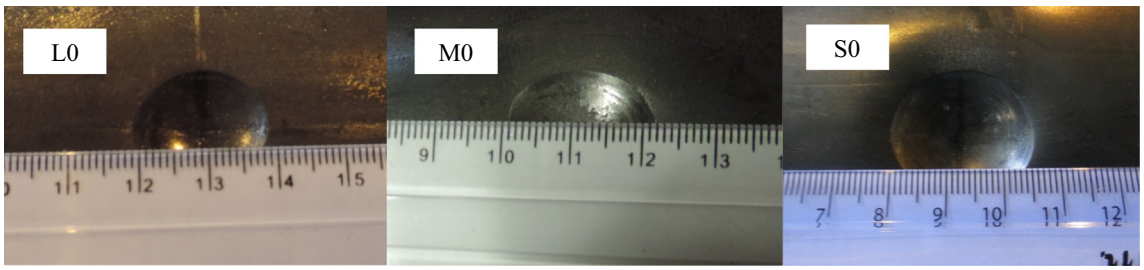

(a) The effect of the specimen length

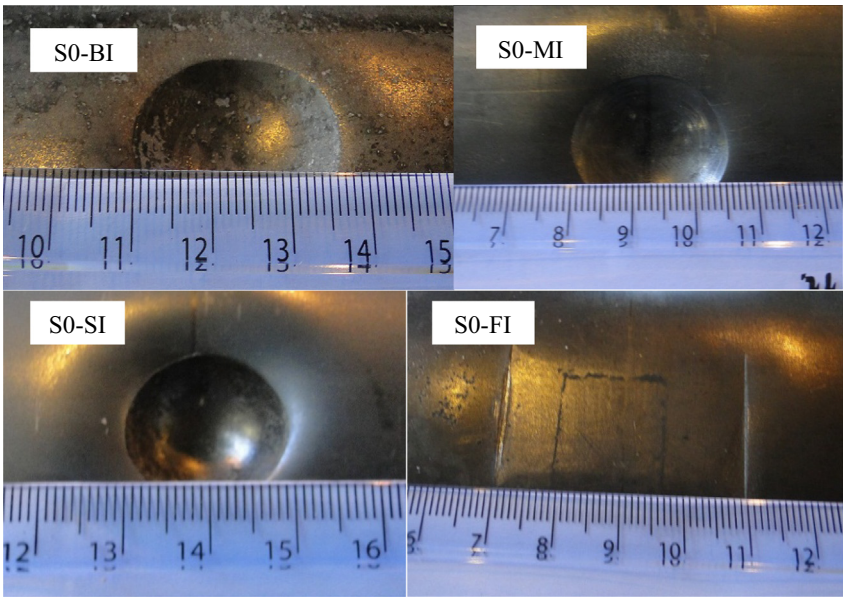

(b) The effect of the impactor shape and diameter

Fig. 11. Deformation modes of specimens. (a) The effect of the specimen length. (b) The effect of the impactor shape and diameter.

$$A_2 = 1.7 \quad \text{for } \frac{L}{D} \leqslant 6 \tag{6}$$

Due to the limited experimental results available on the flat impactor with $L/D > 6$ and the wedge impactor, no shape factor is provided in this study to cover impactors with this ratio range. The modified model is applicable for the circular CFST column with fixed ends only and a further modification is necessary to obtain the maximum displacement for the CFST column with different section shapes, boundary conditions and impactor configurations.The maximum total displacement is further proposed as

$$\delta_{max} = \frac{L \times \mathrm{KE}}{8M_p} A_i \tag{7}$$

Different theoretical models are developed to predict the plastic moment of the CFST. Elchalakani et al. [12] derived a model to calculate the ultimate bending capacity for circular CFSTs. The plastic moment is expressed as

$$M_p = \frac{2}{3} f_c' r_i^3 \cos^3 \gamma_0 + 4 f_y r_m^2 t \cos \gamma_0 \tag{8}$$

where f_c' is the compressive strength of concrete cylinder, f_y is the yield strength of steel tube, t is the tube thickness, r_i is the inner radius of the tube, and $r_m = (r_i + R)/2$ is the mean radius. γ_0 is the angular location of the plastic neutral axis and it can be calculated by the following equation.

$$\gamma_0 = \frac{\frac{\pi}{4}\left(\frac{f_c' r_i^2}{f_y r_m t}\right)}{2 + \frac{1}{2}\left(\frac{f_c' r_i^2}{f_y r_m t}\right)} \tag{9}$$

Deng et al. [44] calculated the moment capacity of the CFST columns by the summation of the constituent moments of the steel and concrete about the neutral axis. Other formulae to calculate the plastic moment were developed by Han [10], Roeder [45], CIDECT [46] and the AIJ code [47]. All these formulae are employed in Eq. (7) to predict δ_{max} and the calculated displacements are compared with the experimental data to evaluate different approaches. The full comparisons of the experimental measurements and those predicted using the current modified model based on various plastic moment formulations are listed in Table 3. Fig. 17 shows the predicted maximum displacements using Eq. (7) with the plastic moment model from Elchalakani et al. [12], together with the experimental data. It is clear that the predicted δ_{max} values are in a very good agreement with the experimental results, in relation to different parameters, i.e. tube thickness, L/D, D/d_i and concrete type.

Some research work [11,33,34] included the strain rate effect for steel using the Cowper–Symonds model and for concrete in tension and compression using the relationships given in the CEB-FIP model code [48].

Although some researchers [49] indicated that there is an insignificant strain rate effect on impact tests with a strike velocity

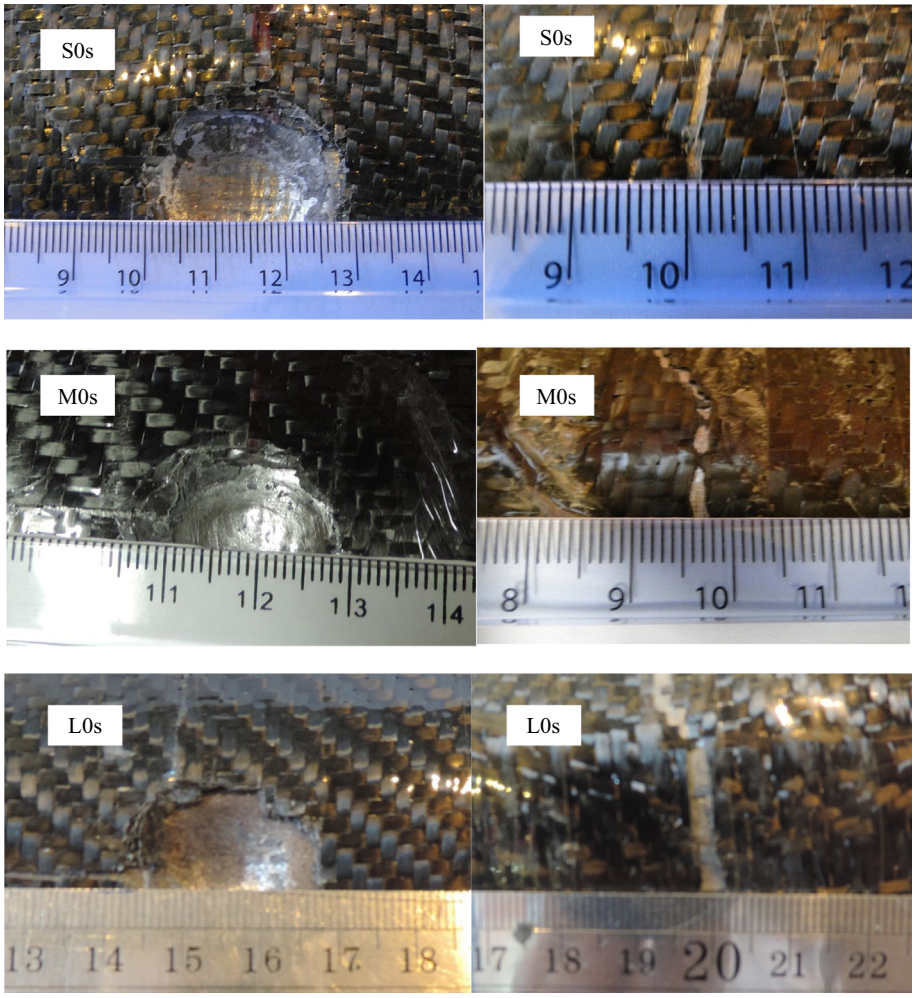

Fig. 12. The effect of the specimen length on the failure mode of the specimens strengthened with FRP.

less than 10 m/s, according to Deng and Tuan [36] such the effect (resulting in 10–20% increase of the material strengths) cannot be ignored in the analysis and design of concrete and steel even subjected to lateral impact with such the velocity. However, the current analysis is based on the static moment capacity. Therefore, it is worth pointing out that the theoretical predictions of impact force and the related displacement may only be valid to the cases related to the following parameter ranges, i.e. an impact velocity up to 10 m/s; concrete strength: 20–80 MPa; yield strength of steel: 250–750 MPa; D/t ratio: 23–83.

4.2. Impact force

Bambach [31] presented a theoretical model to predict the maximum force for the CFST member with fixed ends under static and impact loadings based on a rigid-plastic analysis, which may be expressed as

$$F = \frac{6M_p}{L}\left(\frac{N_0\delta_{max}}{4M_p}\right)^2 + \frac{8M_p}{L} \tag{10}$$

where N_0 is the fully plastic axial force of the steel tube and it can be calculated from:

$$N_0 = 4Dtf_y \tag{11}$$

This model is applicable to L/D ratios between 14 and 35. Therefore, a modification was required to use this model suitable for the short circular CFST columns. The modified model is proposed as:

$$F = \left(\frac{6M_p}{L}\left(\frac{N_0\delta_{max}}{4M_p}\right)^2 + \frac{8M_p}{L}\right) \times B \times C \tag{12}$$

where B and C are the modification factors obtained from a regression analysis based on the current experimental results, which can be obtained from:

$$B = \begin{cases} 0.002 * \left(\frac{L}{D}\right)^2 + 0.0179 * \frac{L}{D} + 0.5416, & \text{for } 3 < \frac{L}{D} < 14 \\ 1.2, & \text{for } \frac{L}{D} \geqslant 14 \end{cases} \tag{13}$$

$$C = \begin{cases} 0.77209 * \frac{d_i}{D} + 0.69, & \text{for spherical impactors} \\ 1.2, & \text{for flat impactors} \end{cases} \tag{14}$$

For the wedge and flat impactor with $L/D > 6$, the factor "C" is not applicable due to the limited experimental results available. Thus the impact force for the specimens, tested by Wang et al. [37] and Han et al. [35], was predicted based on their experimental maximum displacement. These results, together with the impact force predicted for the CFST specimens of the current study, are compared with the experimental data. The comparison has shown a

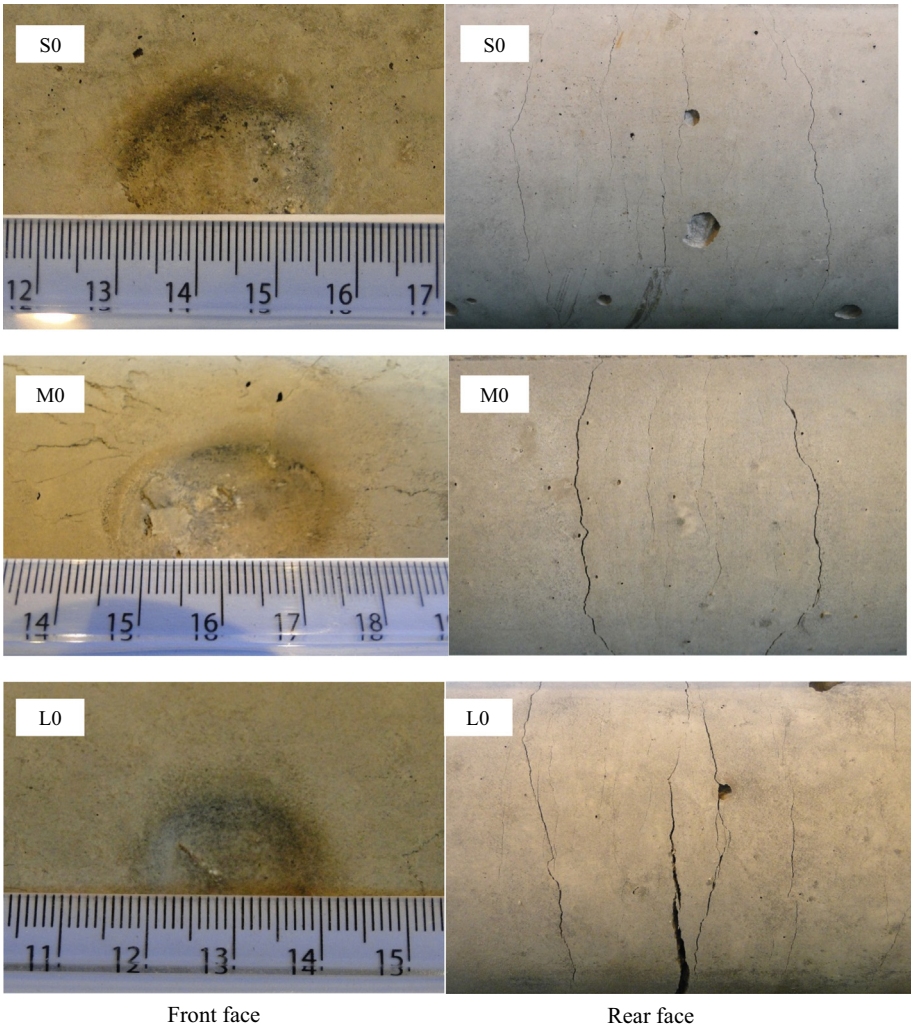

Fig. 13. The effect of the specimen length on the failure mode of the concrete core of the CFST specimens.

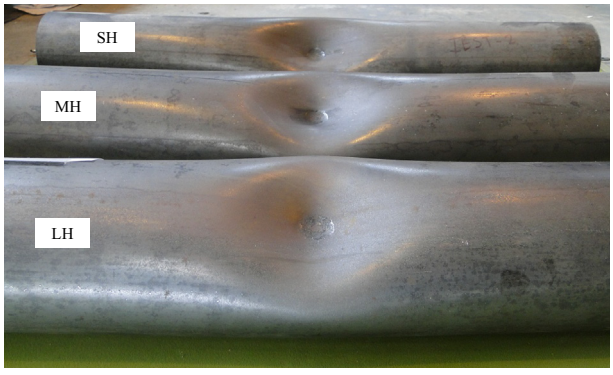

Fig. 14. The effect of the specimen length on the failure mode of the hollow specimens.

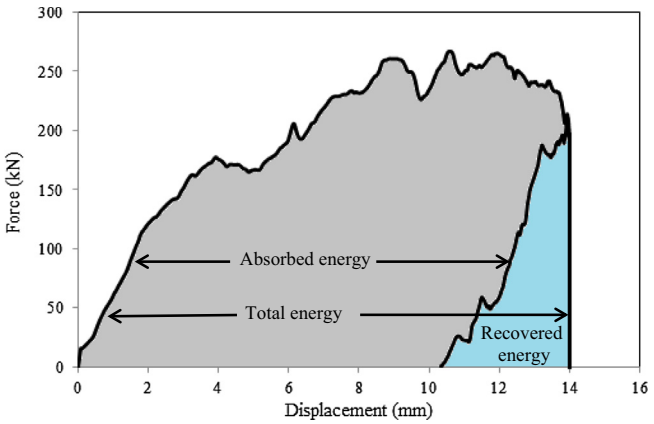

Fig. 15. The calculation of the total and absorbed energies for the short NACFST column.

very good agreement between the recorded impact force and those predicted using the modified model, which is displayed in Fig. 18. The complete comparison between the experimental impact force and the predicted ones using Eq. (13) with different plastic moment models is summarised in Table 4. It shows that the predicted impact forces with the closest correlation to the experimental ones were obtained by employing the plastic moment calculation proposed by Elchalakani et al. [12]. The modified model was also validated against the results from Han et al. [35] and Wang et al. [37]. Table 5 compares the predicted impact forces with the measured ones for the specimens from those experimental studies. The modified model is applicable for the circular CFST columns with fixed ends only and further work is required to compute the maximum impact

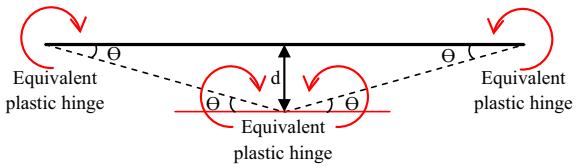

Fig. 16. Equivalent plastic hinge model for the fixed ends CFST column.

force for the CFST column with different tube cross sections, boundary conditions and impactor shapes.

4.3. Influence of various parameters

Using the modified models developed in this paper, parametric studies were carried out on the selected parameters that may affect the impact behaviour of CFST under lateral impact loadings. The predicted results are listed in Table 6.

4.3.1. The tube length

The effect of the length to diameter ratio of the tube was studied, which is shown in Fig. 19. The adopted ratios were from 6 to 40. The results show that with increasing the tube length, the displacement increases from 31.5 mm to 94.4 mm. However, the impact force decreases from 144 kN to 69 kN. This is due to the reduction of the tube stiffness with increasing slenderness.

4.3.2. The material strength

Effects of both the concrete compressive strength and yield strength of the steel tube on the impact response were also studied (Table 6). The results show that increasing the compressive strength of the concrete from 20 MPa to 80 MPa leads to an increase in the impact force from 146.3 kN to 171.5 kN, whilst it reduces the total displacement from 32.2 mm to 26.6 mm. The total displacement is reduced by 59.2% and the impact force increased by 133% with increasing the yield strength f_y from 250 MPa to 750 MPa, due to the increase of the plastic moment

Table 3
The comparison between the predicted total displacements from Eq. (7) for the CFST columns using different plastic moment models.

Tube ID	Exp. dis. (mm)	Pred. dis. (mm) (1)	Error % (1)	Pred. dis. (mm) (2)	Error % (2)	Pred. dis. (mm) (3)	Error % (3)	Pred. dis. (mm) (4)	Error % (4)	Pred. dis. (mm) (5)	Error % (5)
S0-MI	14.0	15.3	9.3	17.1	22.4	16.2	15.7	11.5	17.7	17.3	23.6
S50-MI	14.6	15.4	5.4	17.1	17.3	16.1	10.4	11.5	21.4	17.2	17.7
S0s-MI	13.9	14.3	3.1	16.0	15.5	15.2	9.2	10.8	22.4	16.2	16.6
S50s-MI	14.0	14.1	0.8	15.7	12.2	14.8	5.6	10.5	24.9	15.8	12.6
S0-BI	12.9	13.3	2.7	14.8	15.0	14.0	8.8	10.0	22.6	15.0	16.2
S50-BI	13.4	13.4	0.0	14.9	11.3	14.0	4.7	10.0	25.5	15.0	11.7
S0-SI	16.4	16.9	2.8	18.9	15.1	17.9	8.9	12.7	22.6	19.1	16.3
S50-SI	15.6	16.7	6.8	18.5	18.8	17.4	11.8	12.4	20.4	18.6	19.3
S0-FI	11.2	11.3	1.1	12.7	13.2	12.0	7.0	8.5	23.9	12.8	14.3
S50-FI	11.4	11.5	0.4	12.7	11.7	12.0	5.2	8.5	25.2	12.8	12.1
M0	18.8	19.7	4.6	22.0	17.0	20.8	10.5	14.8	21.4	22.2	18.0
M50	19.2	20.2	5.1	22.4	16.8	21.1	9.8	15.0	21.8	22.5	17.0
M0s	19.2	18.0	6.1	20.2	5.0	19.0	0.8	13.5	29.5	20.3	5.9
M50s	18.6	18.1	2.5	20.1	8.2	18.9	1.8	13.5	27.5	20.2	8.5
L0	28.2	29.2	3.4	32.5	15.3	30.6	8.7	21.8	22.7	32.7	16.0
L50	29.8	30.5	2.4	33.8	13.3	31.7	6.4	22.6	24.2	33.8	13.4
L0s	29.0	27.5	5.3	30.6	5.5	28.8	0.5	20.5	29.2	30.8	6.1
L50s	28.0	27.4	2.3	30.3	8.2	28.4	1.5	20.3	27.7	30.3	8.2
S0	19.0	20.3	6.7	19.9	4.6	21.9	15.4	15.8	16.9	24.0	26.1
S50	19.4	20.3	4.8	19.8	2.2	21.8	12.4	15.7	19.1	23.8	22.5
S0s	20.8	20.2	3.1	19.8	5.0	21.8	4.9	15.7	24.5	23.8	14.5
S50s	19.9	19.5	1.8	19.0	4.3	21.0	5.3	15.1	24.2	22.8	14.8

Where: "(1)", "(2)", "(3)", "(4)", and "(5)" refer to the predicted total displacements based on the plastic moment models from Elchalakani et al. [12], Han, CIDECT [45], AIJ [46], and Roeder et al. [44], respectively.

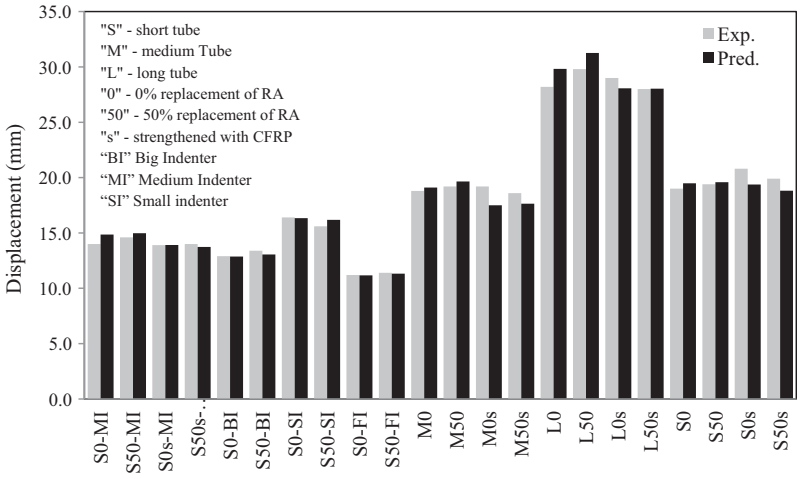

Fig. 17. Comparison between the experimental and predicted maximum total displacement for the CFST columns with different parameters.

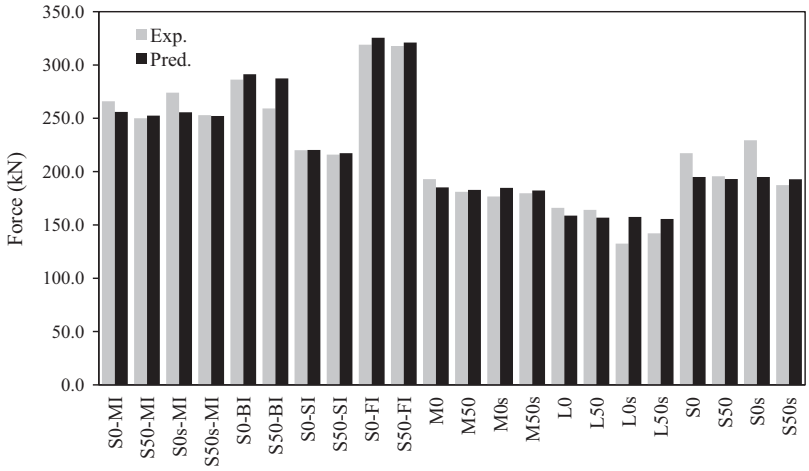

Fig. 18. Comparison between the experimental and predicted impact force for the CFST columns with different parameters.

Table 4
The comparison between the predicted impact force from Eq. (12) for the CFST columns using different plastic moment models.

Tube ID	Exp. F (kN)	Pred. F (kN) (1)	Error % (1)	Pred. F (kN) (2)	Error % (2)	Pred. F (kN) (3)	Error % (3)	Pred. F (kN) (4)	Error % (4)	Pred. F (kN) (5)	Error % (5)
S0-MI	266.0	258.6	2.8	232.3	12.7	244.9	7.9	341.0	28.2	238.3	10.4
S50-MI	250.0	255.8	2.3	231.3	7.5	244.9	2.1	340.8	36.3	237.0	5.2
S0s-MI	274.0	258.3	5.7	231.9	15.4	244.5	10.8	340.9	24.4	239.3	12.7
S50s-MI	253.0	255.4	0.9	230.7	8.8	244.4	3.4	340.6	34.6	238.2	5.8
S0-BI	286.3	294.2	2.8	263.9	7.8	278.5	2.7	388.7	35.8	274.1	4.3
S50-BI	259.3	291.0	12.2	262.8	1.3	278.5	7.4	388.4	49.8	272.4	5.1
S0-SI	220.1	222.7	1.2	200.3	9.0	211.0	4.1	293.3	33.2	203.3	7.7
S50-SI	216.0	220.2	2.0	199.3	7.7	210.9	2.4	293.0	35.6	202.6	6.2
S0-FI	319.0	312.3	2.1	279.8	12.3	295.4	7.4	413.2	29.5	293.5	8.0
S50-FI	317.8	308.9	2.8	278.6	12.3	295.4	7.0	412.8	29.9	291.6	8.2
M0	193.0	186.7	3.3	168.5	12.7	177.4	8.1	245.5	27.2	169.8	12.0
M50	181.1	184.7	2.0	167.9	7.3	177.5	2.0	245.3	35.5	168.7	6.8
M0s	176.7	186.1	5.3	167.8	5.0	176.8	0.1	245.3	38.8	171.2	3.1
M50s	179.7	184.1	2.4	167.1	7.0	176.8	1.6	245.1	36.4	170.4	5.2
L0	166.0	160.5	3.3	146.9	11.5	154.0	7.2	209.3	26.1	139.9	15.7
L50	164.1	159.4	2.8	147.0	10.4	154.5	5.8	209.2	27.5	138.5	15.6
L0s	132.5	159.9	20.7	146.0	10.2	153.2	15.7	209.0	57.7	141.7	7.0
L50s	142.1	158.2	11.3	145.3	2.2	153.1	7.7	208.7	46.9	141.7	0.3
S0	217.3	195.8	9.9	200.7	7.6	182.0	16.3	248.6	14.4	173.2	20.3
S50	195.7	194.2	0.8	200.1	2.3	182.0	7.0	248.6	27.0	172.4	11.9
S0s	229.4	195.8	14.7	200.7	12.5	182.0	20.7	248.6	8.4	173.3	24.5
S50s	187.4	193.9	3.5	199.8	6.6	181.6	3.1	248.6	32.7	173.3	7.5

Where: "(1)", "(2)", "(3)", "(4)", and "(5)" refer to the predicted total displacements based on the plastic moment models from Elchalakani et al. [12], Han, CIDECT [45], AIJ [46], and Roeder et al. [44], respectively.

Table 5
Comparisons between the predicted maximum impact force and experimental results from Wang et al. [37] and Han et al. [35].

	Tube ID	Exp. dis. (mm)	Exp. F (kN)	Pred. F (kN)	Error %
Wang et al.	DBF14	19.4	59.5	57.0	4.2
	DBF16	25.7	59.0	57.3	2.8
	DBF17	32.7	60.6	57.8	4.7
	DBF13	41.9	60.8	58.5	3.8
	DBF12	56.1	60.0	60.0	0.0
	DZF32	17.0	102.0	104.7	2.6
	DZF22	39.4	112.8	109.9	2.6
	DZF23	63.8	112.4	120.3	7.0
	DZF24	65.4	112.2	121.1	8.0
	DZF25	72.4	125.2	125.1	0.1
	DZF27	74.0	120.8	126.1	4.4
	DZF28	79.4	122.6	129.5	5.6
	DZF29	82.3	122.8	131.4	7.0
	DZF26	87.2	123.2	134.9	9.5
Han et al.	CC1	64.0	231.0	202.5	12.4
	CC2	70.0	241.0	203.8	15.5
	CC3	91.0	198.0	209.2	5.6

Table 6
The effect of the selected parameters on the maximum impact force and total displacement for CFST columns.

Variables	V (m/s)	f_c' (MPa)	f_y (MPa)	d_i (mm)	t (mm)	D (mm)	L (mm)	L/D	Mass (kg)	Dis. (mm)	F (kN)
L	7	56.7	450	40	3.6	114.3	1500	13.0	106.5	31.5	144.0
							2000	17.5		42.0	119.4
							2500	22.0		52.5	99.5
							3000	26.0		63.0	86.9
							3500	31.0		73.4	78.5
							4000	35.0		83.9	72.8
							4500	40.0		94.4	68.8
d_i	7	56.7	450	80	3.6	114.3	520		106.5	13.6	330.7
				100						13.3	366.9
				120						13.2	403.1
				140						13.0	439.3
				160						13.0	475.5
				180						12.9	511.8
f_c'	7	20	450	40	3.6	114.3	1360		106.5	32.2	146.3
		30								31.1	150.3
		40								30.1	154.4
		60								28.3	162.8
		70								27.4	167.1
		80								26.6	171.5
f_y	7	56.7	250	40	3.6	114.3	1360		106.5	45.1	105.5
			350							35.0	133.5
			550							24.1	189.5
			650							20.9	217.6
			750							18.4	245.8
V	3	56.7	450	40	3.6	114.3	1360		106.5	5.2	156.0
	5									14.6	157.3
	9									47.2	171.2
	12									83.9	204.6
	15									131.0	274.9
Mass	7	56.7	450	40	3.6	114.3	1360		20	5.4	156.0
									50	13.4	157.0
									150	40.2	167.0
									200	53.6	175.7
									250	67.0	186.9
D	7	56.7	450	40	3.6	100	4000		106.5	110.3	74.9
						114.3				83.9	108.2
						150				48.4	106.0
						200				27.1	177.4
						250				17.4	287.6
						300				12.1	433.5
t	7	56.7	450	40	3.6	114.3	4000		106.5	83.9	72.8
					5					65.6	86.8
					6					57.1	96.6
					7					50.8	106.1

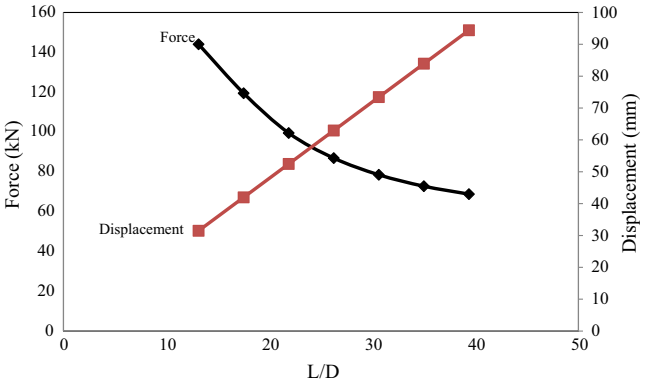

Fig. 19. The effect of the L/D ratio on the maximum total and impact force.

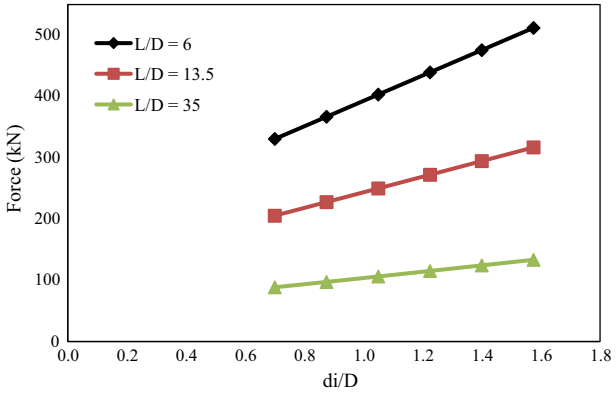

Fig. 20. The effect of the d_i/D ratio on the maximum impact force.

capacity of the column section. Clearly, the change of concrete strength has much less influence on the impact response in comparison to changes of the L/D ratio and the yield strength of the steel tube.

4.3.3. The impactor diameter

The spherical impactor diameter has a significant influence on the impact force, particularly with a small L/D ratio. Fig. 20 shows the increase of the impact force with increasing the impactor

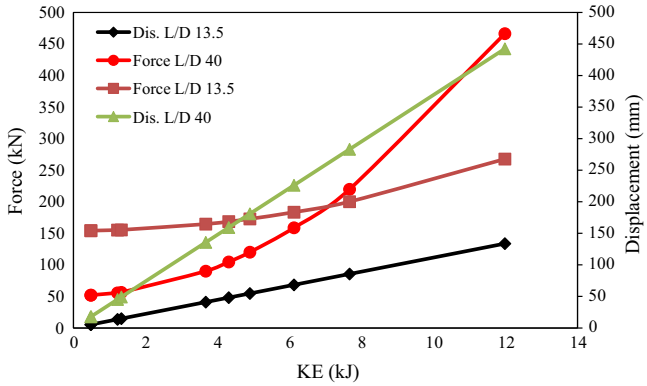

Fig. 21. The effect of the impact kinetic energy on the total displacement and impact force.

diameter from 100 mm to 180 mm with three L/D ratios. Increasing the contact area between the impactor and the tube reduces the local indentation and increases the impact resistance of the columns in a linear fashion for a given L/D ratio.

4.3.4. The impact kinetic energy

Two L/D ratios were selected to examine the influence of the impact kinetic energy on the total displacement and impact force by using a range of impact velocities and drop hammer masses. The impact velocity range was from 3 m/s to 15 m/s, while the drop hammer mass range was from 20 kg to 250 kg. The results show that the KE affects the impact response significantly, particularly with slender columns. When the KE increases, both the total displacement and the impact force increase, especially with high L/D ratio, as shown in Fig. 21. The impact force increases from 52 kN to 466 kN and the displacement increases from 18 mm to 442 mm by increasing the kinetic energy from 0.5 kJ to 12 kJ with L/D ratio equal to 40. Increase of the initial impact energy makes the column dissipate more energy due to increasing the impact force and the corresponding displacement induced by the loading with high strain-rates. The linear displacement and nonlinear force are attributed to a linear function of the KE for the former and a quadratic function of the KE for the latter.

4.3.5. The thickness and the outer diameter of the tube

Increasing the tube wall thickness and/or the outer diameter will increase the plastic moment capacity due to increasing the moment of inertia of the tube section, which leads to a stiffer column with a higher flexural capacity. This is shown clearly in Table 6, which indicates the effects of the thickness and the outer diameter of the tube on the total displacement and impact force, respectively. The predicted results show that reducing the tube wall thickness from 7 mm to 3.6 mm leads to a reduction of the impact force by 46% and increasing the displacement by 65%. With the same L/D ratio, increasing the tube diameter from 100 mm to 300 mm reduces the total displacement from 110 mm to 12 mm and increases the impact force from 75 kN to 433.5 kN.

5. Conclusions

The structural behaviour of a large number of strengthened and unstrengthened RACFST and NACFST columns subjected to lateral impact loads has been investigated. Different column lengths and impactors with various configurations are studied. In general, the findings show that the RACFST and NACFST specimens have similar deformation modes in relation to a number of parameters, i.e. tube length, type of concrete, impactor diameter and the CFRP reinforcement. The maximum force and the total displacement of the RACFST tubes are comparable to those of the NACFST counterparts due to the comparable compressive strengths of both types of concrete. The results also indicate that the load carrying capacity is reduced by 27% and 38% when the tube length increased from 686 mm to 1543 mm, respectively. The unfilled reference steel tubes with different lengths are also subjected to impact loading to study the effect of the concrete filling on the impact behaviour. The concrete filling has significantly enhanced the impact and the total indentation resistance as well as reduced the global displacement. The impactor configurations significantly affect the impact force and the displacement for the tubes filled with normal and recycled aggregate concrete. Enlarging the spherical diameter from 20 mm to 60 mm increases the impact force from 220 kN to 286 kN and reduces the indentation depth from 10.2 mm to 4.6 mm.

The CFRP plays an effective role in enhancing the resistance to global displacement. One layer of the CFRP reinforcement has reduced the global displacement by about 8.3% and 6.2% for the long and medium tubes, respectively. The RACFST tube can be recommended as a structural composite member for construction due to the comparable load carrying capacity to the NACFST tube and conservation of the natural resources, with appropriate mechanical properties of the recycled aggregate.

The modified theories have been proposed to predict the total displacement and the impact force of the concrete filled steel tube columns studied. The predicted results have shown a very good agreement with those recorded from the experimental investigation. With the validated models, the parametric studies have been undertaken to provide reasonable results on influence of different parameters such as L/D ratio, d_i/D ratio, tube thickness, material properties and the impact energy on the impact response. Here, with increasing the L/D ratio from 13 to 40, the impact force is decreased from 144 kN to 69 kN, whilst the displacement increased from 31 mm to 94 mm. The CFST column exhibits a higher impact resistance with increasing the d_i/D ratio for a given L/D ratio. Increasing the tube wall thickness from 3.6 mm to 7 mm shows a significant effect on the impact response of the CFST columns, with the impact force being increased from 73 kN to 106 kN and the displacement being reduced from 84 mm to 51 mm. For the non-perforation damage, increasing the kinetic energy by increasing the impact velocity and the drop hammer mass induces the CFST column to increase the impact resistance and the energy dissipation. The higher concrete strength and steel tube strength contribute to the increase of the impact force and the decrease of the displacement due to the high flexural capacity of the tube.

Acknowledgements

The work presented in this paper was supported by the Higher Committee for Education Development (HCED) in Iraq. The authors would like to thank Sloyan Doyle demolition company (Liverpool, England), for providing the recycled aggregate. The authors also would like to thank Dr. R. Birch for his help with the data processing.

References

[1] Shanmuam NE, Lakshmi B. State of the art report on steel–concrete composite columns. J Constr Steel Res 2001;57:1041–80.
[2] He D, Dong J, Wang Q, Chen X. Mechanical behaviour of recycled concrete filled steel tube columns strengthened by CFRP. In: International Conference on Multimedia Technology (ICMT). Hangzhou: IEEE; 2011. p. 1110–3.
[3] Sundarraja MC, Prabhu GG. Investigation on strengthening of CFST members under compression using CFRP composites. J Reinf Plast Compos 2011;30:1251–64.
[4] Morino S, Uchikoshi M, Yamaguchi I. Concrete-filled steel tube column system-its advantages. Int J Steel Struct 2001;1(1):33–44.

[5] Morino S, Tsuda K. Design and construction of concrete-filled steel tube column system in Japan. Earthq Eng Eng Seismol 2002;4(1):51–73.
[6] Starossek U, Falah N, Loehning T. Numerical analyses of the force transfer in concrete-filled steel tube columns. Struct Eng Mech 2010;35(2):241–56.
[7] Kang JY, Choi ES, Chin WJ, Lee JW. Flexural behavior of concrete-filled steel tube members and Its application. Int J Steel Struct 2007;7:319–24.
[8] Jiang SF, Wu ZQ, Niu DS. Experimental study on fire-exposed rectangular concrete-filled steel tubular (CFST) columns subjected to bi-axial force and bending. Adv Struct Eng 2010;13:551–60.
[9] Gho WM, Liu D. Flexural behaviour of high-strength rectangular concrete-filled steel hollow sections. J Constr Steel Res 2004;60:1681–96.
[10] Han L. Flexural behaviour of concrete filled steel tubes. J Constr Steel Res 2004;60(2):313–37.
[11] Deng Y, Tuan CY, Xiao Y. Flexural behavior of concrete-filled circular steel tubes under high-strain rate impact loading. J Struct Eng 2012;138:449–56.
[12] Elchalakani M, Zhao XL, Grzebieta RH. Concrete-filled circular steel tubes subjected to pure bending. J Constr Steel Res 2001;57:1141–68.
[13] Yang YF, Han LH, Wu X. Concrete shrinkage and creep in recycled aggregate concrete-filled steel tubes. Adv Struct Eng 2008;11:383–96.
[14] Chen ZP, Chen XH, Ke XJ, Xue JY. Experimental study on the mechanical behavior of recycled aggregate coarse concrete-filled square steel tube column. In: International Conference on Mechanic Automation and Control Engineering (MACE). Wuhan: IEEE; 2010. p. 1313–6.
[15] Wu B, Zhao XY, Zhang JS. Cyclic behaviour of thin-walled square steel tubular columns filled with demolished concrete lumps and fresh concrete. J Constr Steel Res 2012;77:69–81.
[16] Yang Y, Ma G. Experimental behaviour of recycled aggregate concrete filled stainless steel tube stub columns and beams. Thin Walled Struct 2013;66:62–75.
[17] Dong JF, Wang QY, Guan ZW. Structural behaviour of recycled aggregate concrete filled steel tube columns strengthened by CFRP. Eng Struct 2013;48:532–42.
[18] Yang YF, Han LH. Experimental behaviour of recycled aggregate concrete filled steel tubular columns. J Constr Steel Res 2006;62:1310–24.
[19] Yang YF, Han LH, Zhu LT. Experimental performance of recycled aggregate concrete-filled circular steel tubular columns subjected to cyclic flexural loadings. Adv Struct Eng 2009;12:183–94.
[20] Teng JG, Lam L. Behavior and modeling of fiber reinforced polymer-confined concrete. J Struct Eng 2004;130:1713–23.
[21] Sundarraja MC, Prabhu GG. Experimental study on CFST members strengthened by CFRP composites under compression. J Constr Steel Res 2012;72:75–83.
[22] Prichard SJ, Perry SH. The impact behaviour of sleeved concrete cylinders. Struct Eng 2000;78(17):23–7.
[23] Shan JH, Chen R, Zhang WX, Xiao Y, Yi WJ, Lu FY. Behavior of concrete filled tubes and confined concrete filled tubes under high speed impact. Adv Struct Eng 2007;10:209–18.
[24] Huo J, Zheng Q, Chen B, Xiao Y. Tests on impact behaviour of micro-concrete-filled steel tubes at elevated temperatures up to 400 °C. Mater Struct 2009;42:1325–34.
[25] Cui XG, Xu HD. Analysis of uniaxial dynamic performance of concrete-filled square steel tube composite column. Appl Mech Mater 2011;94:220–4.
[26] Reid SR, Reddy T, Gray MD. Static and dynamic axial crushing of foam-filled sheet metal tubes. Int J Mech Sci 1986;28(5):295–322.
[27] Xiao Y, Shan J, Zheng Q, Chen B, Shen Y. Experimental studies on concrete filled steel tubes under high strain rate loading. J Mater Civ Eng 2009;21:569–77.
[28] Chakradhara M, Bhattacharyya SK, Barai SV. Behaviour of recycled aggregate concrete under drop weight impact load. Constr Build Mater 2011;25:69–80.
[29] Xiaoqing M, Stronge WJ. Spherical missile impact and perforation of filled steel tubes. Int J Impact Eng 1985;3(1):1–16.
[30] Nishida M, Tanaka K. Experimental study of perforation and cracking of water-filled aluminium tubes impacted by steel spheres. Int J Impact Eng 2006;32 (12):2000–16.
[31] Bambach MR, Jama H, Zhao XL, Grzebieta RH. Hollow and concrete filled steel hollow sections under transverse impact loads. Eng Struct 2008;30:2859–70.
[32] Bambach MR. Design of hollow and concrete filled steel and stainless steel tubular columns for transverse impact loads. Thin Walled Struct 2011;49 (10):1251–60.
[33] Qu H, LI G, Chen S, Sun J, Sozen MA. Analysis of circular concrete-filled steel tube specimen under lateral impact. Adv Struct Eng 2011;14:941–52.
[34] Deng Y, Tuan CY. Design of concrete-filled circular steel tubes under lateral impact. ACI Struct J 2013;110(4):24–31.
[35] Han l, Hou C, Zhao X, Rasmussen K. Behaviour of high strength concrete filled steel tubes under transvers impact loading. J Constr Steel Res 2014;92:25–39.
[36] Remennikov AM, Kong SY, Uy B. Response of foam-and concrete-filled square steel tubes under low-velocity impact loading. J Perform Constr Facil 2010;25 (5):373–81.
[37] Wang R, Han L, Hou C. Behavior of concrete filled steel tubular (CFST) members under lateral impact: experimental and FEA model. J Constr Steel Res 2013;80:188–201.
[38] Yousuff M, Uy B, Tao Z, Remennikov AM, Liew R. Behaviour and resistance of hollow and concrete-filled mild steel columns due to transverse impact loading. Aust J Struct Eng 2012;13(1):65–80.
[39] Yousuf M, UY B, Tao Z, Remennikov AM, Liew R. Transverse impact resistance of hollow and concrete filled stainless steel columns. J Constr Steel Res 2013;82:177–89.
[40] Yousuf M, UY B, Tao Z, Remennikov AM, Liew R. Impact behaviour of pre-compressed hollow and concrete filled mild and stainless steel columns. J Constr Steel Res 2014;96:54–68.
[41] British Standards Institution, Testing hardened concrete. Compressive strength of test specimens, BS EN 12390-3; 2009.
[42] Tao Z, Han H, Wang L. Compressive and flexural behaviour of CFRP-repaired concrete-filled steel tubes after exposure to fire. J Constr Steel Res 2007;63 (8):1116–26.
[43] ImPREESSion 6. Necolet Tecnonlgies. Germany: Weisang GmbH & Co. KG.; 2002.
[44] Deng Y, Tuan CY, Zhou Q, Xiao Y. Flexural strength analysis of non-post-tensioned and post-tensioned concrete-filled circular steel tubes. J Constr Steel Res 2011;67(2):192–202.
[45] Roeder C, Lehman D, Bishop E. Strength and stiffness of circular concrete filled tubes. J Struct Eng 2010;136(12):1545–53.
[46] Bergmann R, Matsui C, Meinsma C, Dutta D. CIDECT design guide for concrete filled hollow section columns under static and seismic loading. Verlag, TUV Rheinland; 1995.
[47] (AIJ). Standard for structural calculation of steel reinforced concrete structure. Tokyo: Architectural Institute of Japan; 2001.
[48] Comite Euro-International du Beton. CEB-FIP model code 1990. Trowbridge, Wiltshire, UK: Redwood Books; 2001.
[49] Wang Y, Qian X, Liew JR, Zhang MH. Experimental behavior of cement filled pipe-in-pipe composite structures under transverse impact. Int J Impact Eng 2014;2014(72):1–16.